Life Sciences 239 (2019) 116891

Contents lists available at ScienceDirect

Life Sciences

journal homepage: www.elsevier.com/locate/lifescie

Synergistic effects of adipose-derived stem cells combined with decellularized myocardial matrix on the treatment of myocardial infarction in rats

Liang Qiao[1], Yan Kong[1], Yingshen Shi[1], Aijun Sun, Ruijuan Ji, Chao Huang, Yuquan Li**, Xiangqun Yang*

Department of Anatomy, Institute of Biomedical Engineering, Naval Medical University, Shanghai, 200433, China

ARTICLE INFO

Keywords:
Adipose-derived stem cells (ADSCs)
Decellularized extracellular matrix (dECM)
Myocardial infarction
Cardiac function

ABSTRACT

Aims: The aims of the study are to investigate whether the combination of adipose-derived stem cells (ADSCs) with decellularized extracellular matrix (dECM) of myocardium can exert synergistic therapeutic effects on acute MI and the underlying mechanism.

Main methods: Myocardial dECM from fresh porcine myocardium was prepared in an injectable gel, ADSCs were seeded into the myocardial dECM gels, and then the mixture was injected into the myocardium of the infarct border zone after acute MI, which was induced by ligating the left anterior descending coronary artery in male SD rats, to assess the therapeutic potential. The degree of fibrosis was detected by Masson's trichrome. The evaluation of cardiac function was performed by Electrocardiography.

Key findings: Myocardial dECM (2.0%) had a suitable aperture and arrangement for cell growth, and also exhibited suitable biomechanical properties. Four-weeks after treatment *in vivo*, the combination of ADSCs and myocardial dECM could obviously increase angiogenesis, reduce the degree of fibrosis, and decrease infarct size. Furthermore, the combination treatment exerted significant functional improvement. Compared with ADSCs or dECM group alone, the left ventricular ejection fraction (LVEF) in the combination group was 13.4% and 21.8% elevated, respectively.

Significance: The combination of ADSCs and myocardial dECM has synergistic effects on cardiac repair in acute MI.

1. Introduction

Myocardial infarction (MI), which is known as one of the most prevalent causes of mortality, can result in significant cardiomyocyte loss, myocardial systolic weakness, and eventually heart failure [1,2]. The current strategies of MI treatment are insufficient for controlling its progression because of the limited regenerative capacity of the adult myocardium. Due to their multi-lineage differentiation capacity and paracrine function, exogenous stem cell transplantation is a potential strategy for repairing damaged cardiac tissue [3,4]. Cumulative research has indicated that adipose-derived stem cells (ADSCs) are ideal seed cells for MI because they are easily obtained and expanded, and share multi-potent differentiation properties [5,6]. ADSC transplantation preserved cardiac contractile function and suppressed ventricular tachyarrhythmias in a rat MI model [7]. Intracoronary injection of cultured ADSCs could also improve myocardial perfusion in a porcine acute MI model [8]. Biomaterials, which can provide an adequate three-dimensional scaffold to support the viability and attachment of transplanted cells, had been widely used in heart tissue engineering. In a previous study, brown ADSCs delivered by chitosan hydrogels prevented adverse matrix remodeling, increased angiogenesis, and preserved heart function [9]. Also, porous nanofibrous poly (L-lactic acid) scaffolds supported cardiovascular progenitor cells for cardiac tissue engineering [10], and Isl1 + cardiac progenitor cell transplantation in small intestinal submucosa improved cardiac function, decreased the left ventricular myocardial scarring area, and reduced fibrosis [11]. Furthermore, transplantation of adipose-derived stem cells combined with neuregulin-microparticles favored a synergy function for

* Corresponding author.
** Corresponding author.
E-mail addresses: liyuquanf@163.com (Y. Li), yangxq_sh@126.com (X. Yang).
[1] Authors equally contributed to this article.

https://doi.org/10.1016/j.lfs.2019.116891
Received 13 July 2019; Received in revised form 9 September 2019; Accepted 19 September 2019
Available online 12 October 2019
0024-3205/

promoting efficient cardiac repair in heart regeneration [12].

Natural extracellular myocardial matrix is particularly important for stimulating cell recruitment, attachment, migration and cross-talk with resident cells [13]. As a specific myocardial acellular scaffold material, this kind of decellularized extracellular matrix (dECM) exerted promising cell support ability and myocardial matching mechanical properties [14–16]. Singelyn et al. [17] proved that dECM with low immunogenicity played an active role in repairing MI after injection into infarct heart tissues. Acellular matrix maintains main ECM components and can mimic the native heart ECM biological and chemical cues [18,19]. However, it is unknown whether myocardial dECM can improve the therapeutic effect of ADSCs transplantation and enhance cardiac function in acute MI. In this study, we optimized the procedure for generating dECM from porcine ventricular myocardium and then focused on the hypothesis that myocardial dECM and ADSCs have synergistic effects on MI treatment.

2. Materials and methods

All animal procedures were permitted by the Animal Care and Use Committee of Naval Medical University (permit number SYXK-2002-042). Male Sprague-Dawley (SD) rats and porcine hearts were purchased from the Animal Center of Naval Medical University (Shanghai, China).

2.1. Preparation of solubilized myocardial dECM for gelation

Fresh porcine hearts were rinsed and then the atrium, right ventricle, and epicardium of the left ventricle were removed. The retained myocardium was cut into $2 \times 2 \times 1\ mm^3$ pieces and then rinsed, homogenized, and centrifuged. The supernatant was discarded, and the pelletized cells were decellularized by adding 1% SDS (Sigma, USA) with gentle shaking at 4 °C. SDS was changed every 8 h for 3 days. Decellularized cardiac tissue was centrifuged, and the supernatant was discarded, the remains were rinsed repeatedly in sterile distilled water, freeze-dried, and grounded. Finally, the myocardial dECM powder was harvested (Fig. 1A).

To fabricate an injectable hydrogel, the myocardial dECM powder was digested in a tube with 0.01 M HCl containing pepsin (Sigma, USA) for 6 h at 35.5 °C with constant shaking; the ratio of pepsin: myocardial dECM powder was 1:5 for dissolution [17]. The digestive process consisted of transformation from an unambiguous liquid to a stagnant state, then gradual progression into a flowing and viscous myocardial dECM solution. After uniform digestion, the tube was placed on ice, 10 × PBS was added to adjust the ion balance, 1 M NaOH solution was added up to pH 7.4 to terminate digestion. The liquid flowing in the tube could be changed into solid heat-crosslinked dECM gel after being maintained at 37 °C for 5 min (Fig. 1A, Video 1, and Video 2). Three different myocardial dECM concentrations (1.5%, 2.0%, and 2.5%; w/v) were prepared for subsequent experiments.

Supplementary video related to this article can be found at https://doi.org/10.1016/j.lfs.2019.116891.

2.2. Characterization and biomechanical properties evaluation of myocardial dECM

Normal porcine ventricular and myocardial dECM tissues were embedded in OCT freezing medium, sectioned into 5 μm slices, and then stained with hematoxylin and eosin (H&E). Samples also were underwent immunohistochemical examination under a microscope (Leica Microsystems GmbH, Germany) to identify the following components: type I collagen, type III collagen and laminin.

Different myocardial dECM concentrations were prepared and molded into a $1 \times 1 \times 1\ mm^3$ cylindrical structure for microstructure observation via cryogenic scanning electron microscopy (SEM, FEI, USA).

Moreover, samples were tested respectively using an Instron 4455 universal material testing machine (Biomedical center, Dong Hua University) for stress-strain analysis. The elastic modulus was calculated according to the slope of the ascent.

2.3. ADSC isolation, identification, and differentiation

ADSCs were obtained from the bilateral inguinal adipose tissue of SD rats (60 ± 10 g), and digested in Dulbecco's modified Eagle's medium (DMEM, Corning, USA), containing 0.1% collagenase type II (Sigma, USA) and 1% BSA (MP, USA), for 1 h at 37 °C. The digested tissue was filtered and centrifuged at 1000 rpm for 5 min. The cells were then collected and cultured in DMEM supplemented with 10% fetal bovine serum (Gibco, USA) and 1% penicillin/streptomycin (Gibco, USA) at 37 °C and 5% CO_2 [20,21]. The third generation of ADSCs was used for experiments.

The expression of ADSC immunophenotypes, including CD34, CD29, CD45, and CD90 (Abcam, UK), was evaluated by flow cytometry (BD, USA). ADSCs were cultured in six-well plates at a density of 5×10^5 cells/well, and then the capacity of ADSCs to differentiate into adipocytes, chondrocytes and osteoblasts was determined. Cell differentiation into adipocytes was induced for 10 days, and into chondrocytes and osteoblasts, for 21 days (Cyagen Biosciences Inc., USA). After completion of induced differentiation, the cells were fixed with 4% paraformaldehyde for 10 min, and rinsed with sterile PBS. Further, the following stains were utilized: Oil red O, Alcian blue and Alizarin red (Cyagen Biosciences Inc., USA) for 10 min, respectively, and observed via a microscope (Leica Microsystems GmbH, Germany).

2.4. Assessment of biocompatibility of the myocardial dECM

Three different concentrations of myocardial dECM solution (1 ml) were each mixed with ADSCs (5×10^6) and then maintained undisturbed at 37 °C for 5 min for gelation. They were then cut into 100 μm slices, placed in six-well plates, and cultured for 3 and 7 days. Cell survival and morphology in myocardial dECM was detected by LIVE/DEAD cell viability assay kit (Life Technologies, UK) and laser confocal microscopy (Leica, Germany).

ADSCs seeded in three myocardial dECM concentrations and then were cultured in a 96-well plate. The same number of ADSCs seeded without myocardial dECM was cultured as a control group. The growth and proliferation of cells in cultures with different myocardial dECM concentrations were measured at the time of inoculation 0, 3, and 7 days via the CCK8 assay at OD 450 nm (CCK8, Dojindo, Japan).

2.5. Establishment of acute MI model and ADSCs implantation

Male SD rats (230 ± 10 g) were subjected to permanent MI surgery by ligating the left anterior descending (LAD) coronary artery with a 7-0 silk suture [22]. A week later, the success of MI surgery was confirmed by ST-segment elevation in an electrocardiogram (Supplemental Material Fig. 2B), and then these rats were randomized into 5 groups with different treatments: (1) sham operation (suture placement without occlusion of the coronary artery and treatment, n = 18); (2) MI, injection with PBS (n = 18); (3) PBS + ADSCs, injection with ADSCs suspended in PBS (n = 18); (4) dECM, injection with myocardial dECM solution (n = 18); and (5) dECM + ADSCs, injection of ADSCs seeded in myocardial dECM solution (n = 18). ADSCs (1×10^6) were suspended in 150 μl PBS or myocardial dECM solution, and the mixed solutions were rapidly administered into the myocardium in the infarct border zone at 4 different sites using a 27-gauge catheter.

2.6. Enzyme-linked immunosorbent assay (ELISA)

Venous blood (2 ml) of a rat was collected one week after treatment. Six serum samples from each group were utilized for TNF-α and IL-10

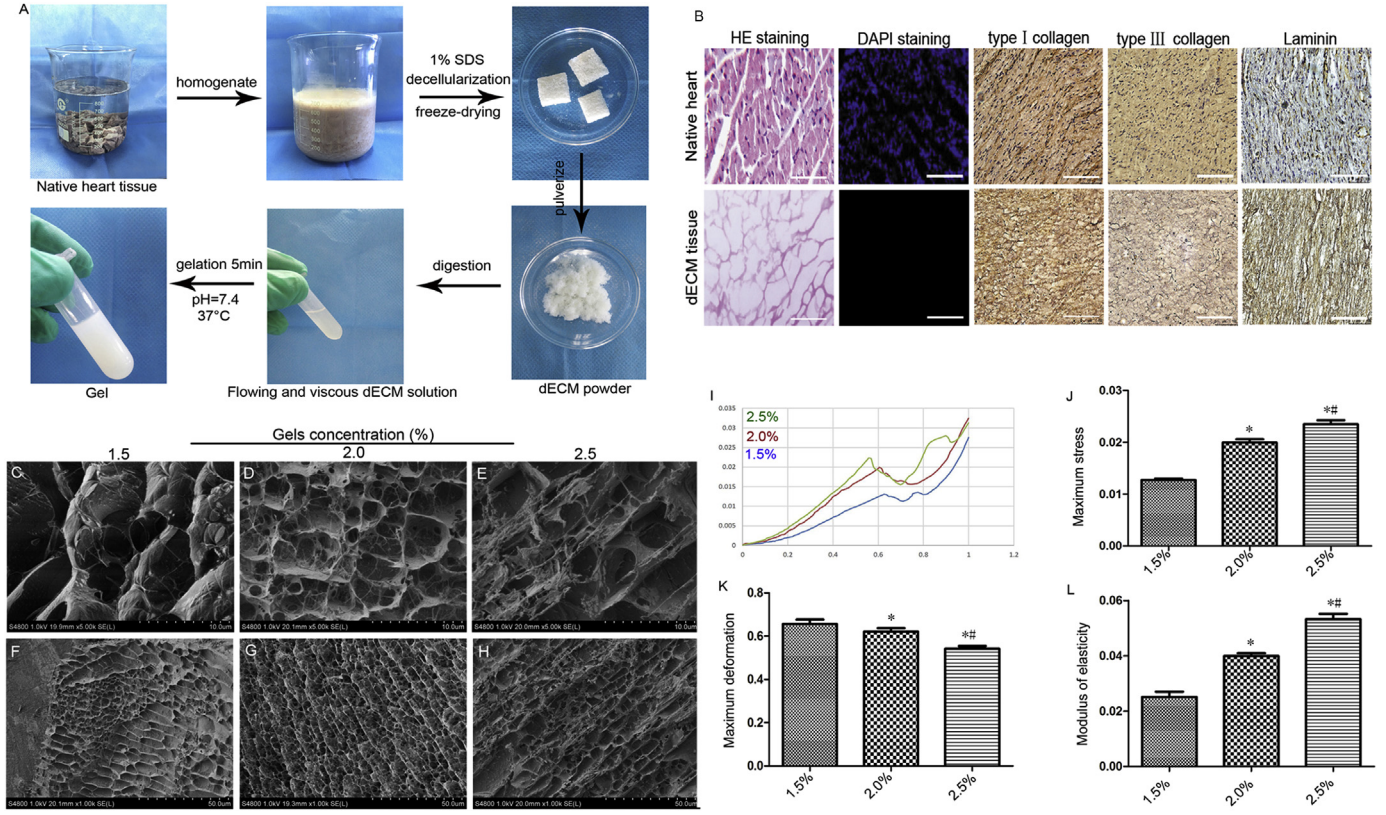

Fig. 1. The preparation and characterization of myocardial dECM. **A.** Preparation of dECM solution for gelation. **B.** The comparison of native heart and myocardial dECM tissues by HE staining and DAPI staining, and component analysis (type I collagen, type III collagen, laminin) by immunohistochemistry. 200×, magnification. **C–H.** Images of myocardial dECM observed using a cryogenic scanning electron microscope. **C-E.** 5000×, magnification, **F–H.** 1000×, magnification. **I-L.** Biomechanical properties evaluation of myocardial dECM in three different concentrations (1.5%, 2.0%, and 2.5%). **I.** Biomechanical curve for stress-strain analysis. **L.** Modulus elasticity was calculated according to the slope of the ascent in Fig. 1**I** (*P < 0.05 vs. 1.5%, #P < 0.05 vs. 2.0%).

analysis via ELISA kits (Wei'ao, Shanghai, China) according to the manufacturer's instruction. The results are shown as mean optical density (OD) values (Supplemental Material Figs. 3A–B).

2.7. Real-time polymerase chain reaction (PCR) analysis

Total RNA was extracted from the heart tissue in the infarct border zone using Trizol reagent. The concentration was determined using a microplate reader, and the RNA was reverse transcribed into cDNA using a Revert Aid First Strand cDNA Synthesis Kit (Thermo Scientific, USA). Real-time PCR was performed using SYBR Green Master Mix (DBI Bioscience, Germany). The relative gene expression was normalized to the internal control GAPDH. Primer sequences of target genes are presented in Table 1.

2.8. Western blotting

Heart tissue from the infarct border zone was obtained after 4 weeks of treatment. The tissues were homogenized on ice, and the supernatant was collected. An equal amount of protein samples, extracted from different groups, was transferred to polyvinylidene difluoride membranes, blocked with 5% non-fat milk in TBST for 1–2 h at room temperature, and incubated overnight at 4 °C with different primary antibodies: Ang-1(1:5000, Abcam, UK), EGF (1:1000, Abcam, UK), VEGF (1:1000, Abcam, UK), and GAPDH (1:2000, Wei'ao, China). The membrane was rinsed with TBST three times and incubated with the secondary HRP-conjugated antibody (1:2000, Jackson, PA, USA) for 1–2 h [23]. The bands were quantified by measuring the band intensity for each group and normalizing to GAPDH, as an internal control, using the Odyssey v1.2 software (LI-COR Biosciences, Lincoln, NE, USA).

Table 1
Primers used in real-time PCR.

Gene name	Forward (5′–3′)	Reverse (5′–3′)
Ang-1	ACAACACCAACGCTCTGCAA	CCATCACATGCTCCAGATGC
VEGF	AGCCTTGTTCAGAGCGGAGA	CCTTGGCTTGTCACATCTGC
EGF	ACGTTGATGAGTGCCAGCAG	AAGGCAGTCCAGGTGCTGAT
GAPDH	GAAGGGCTCATGACCACAGT	GGATGCAGGGATGATGTTCT

Ang-1, angiopoietin-1; VEGF, vascular endothelial growth factor; EGF, epidermal growth factor.

2.9. Histology

Animals were sacrificed 4 weeks after treatment. The hearts were harvested, rinsed with PBS, fixed in 4% buffered formalin, embedded in paraffin, and were cut into sections with 5 μm thickness. All histology sections were stained and analyzed in a blinded manner. Angiogenesis was detected in the section stained with anti-von Willebrand Factor antibody (vWF, 1:400, Abcam). The mean number of vessels was counted in three randomly fields under a microscope at a magnification of × 200 and calculated (n = 3/group).

Masson's trichrome were performed to investigate the cardiac structure and fibrosis after 4 weeks of treatment. The ratio of collagen was calculated by collagen-positive blue area as a percentage of total tissue area via Image J software (n = 3/group).

Some hearts were harvested, and stored at −20 °C for approximately 30 min to harden tissue. Then the hearts were cut into five pieces, stained with 1% TTC (Sigma Aldrich, USA) at 37 °C for 30 min in the dark, fixed in 4% buffered formalin overnight, rinsed with PBS three

times, and then photographed. The pale white area represents infarct tissue, and the dark red region indicates normal heart tissue. Myocardial infarct size was calculated as the ratio of infarct area (pale white area) to the area of the total LV cross-section via the Image Pro Plus software, as previously described [24,25]. The infarct size was averaged and expressed as the mean value of the ratio for each heart (n = 6/group).

2.10. Cardiac function measurement

After implantation for 4 weeks, echocardiography was performed to investigate the left ventricular (LV) function via high-frequency ultrasound system MyLab twice (Esaote, Genova, Italy). Briefly, rats were anesthetized with isoflurane (2.5%) using ventilation equipment, carefully removed fur on the left chest, and then two-dimensional echocardiographic measurements were obtained [26]. Left ventricular internal diastolic and systolic diameter (LVIDd and LVIDs) were measured from M-mode tracing (Left ventricular long axis section). The left ventricular ejection fraction and fractional shortening (LVEF and LVFS) were calculated using the Teichholz method.

Left intraventricular pressure was recorded via right carotid intubation inserted into the LV by Biological Signal Collector (OHAUS, USA), according to the manufacturer's instructions, and the maximal slopes of systolic and diastolic pressure (+dP/dtmax and -dP/dtmin) were analyzed as previously described (n = 7/group) [27].

2.11. Statistical analysis

Statistical analysis was performed through one-way ANOVA analysis with Tukey post-testing using GraphPad Prism5.0 (GraphPad Software, Inc., La Jolla, CA, USA). Data are expressed as means ± SD, and P values < 0.05 were considered significant.

3. Results

3.1. Gelation and characterization of myocardial dECM in vitro

As shown in Fig. 1A, myocardial dECM was successfully prepared. In order to observe the structure of myocardial dECM and determine whether the process of decellularization affects ECM components, native heart and myocardial dECM (before freeze-drying) tissues were compared. As shown in Fig. 1B, the data demonstrated that native heart tissue showed regularly arrayed cardiomyocytes with visible red cytoplasm and blue nuclei, while the myocardial dECM tissue had only some grid structure by HE staining. In addition, there were no blue nuclei remaining in the myocardial dECM tissue by DAPI staining, which also illustrated the successful decellularization. Furthermore, the results demonstrated that there was no significant difference in type I collagen, type III collagen and laminin between the two groups, which indicated that the process of decellularization did not change the primary constituents in the ventricular structure.

To determine the proper concentration for the experiment, 1.5%, 2.0%, and 2.5% myocardial dECM was prepared and analyzed by cryogenic scanning electron microscopy. The 1.5% myocardial dECM demonstrated a large aperture with uneven arrangement (Fig. 1C, F). The 2.5% myocardial dECM had a relatively dense aperture with poor permeability that might inhibit ADSC co-culture (Fig. 1 E, H). However, the 2.0% myocardial dECM showed relatively even aperture and arrangement (Fig. 1D, G).

As shown in Fig. 1I, K, the results indicated that the higher the concentration, the smaller the maximum deformation. The maximum deformations for the three myocardial dECM concentrations were significantly different ($P < 0.05$). However, the maximum stress for the three different concentrations showed an opposite trend compared with maximum deformation (Fig. 1J). Using the rising period shown in Fig. 1I, a line was roughly fitted, and the slope was calculated to determine the elastic modulus of different concentrations for stress-strain analysis. The data indicated that the 1.5% concentration showed poor stress and strain, while the 2.5% hydrogel could withstand greater stress than the other two groups and had the largest elastic modulus (Fig. 1L). Nevertheless, the 2.5% myocardial dECM had a considerably long digestion time and was hard to digest appropriately during the preparing process. Taken together, the 2.0% myocardial dECM demonstrated suitable mechanical properties and was most appropriate for the experiment.

3.2. Characteristics of ADSCs and their multi-lineage potential

ADSCs were harvested, and the cell phenotypes were detected using flow cytometry. The cells were positive for CD29 and CD90 and negative for CD34 and CD45 (Supplemental Material Fig. 1A). The data was in accordance with the phenotypical characteristics of mesenchymal stem cells [28].

After adipogenic induction, the cytoplasm exhibited translucent intracellular lipid droplets in up to 90% of the whole cell confirmed by Oil Red O staining. However, this change was not observed after 10 days of induced differentiation in the control group. Chondrogenesis was confirmed via positive vitriolic proteoglycans. After 21 days of osteogenic induction, the typical calcified nodules with orange color were identified via Alizarin red staining, while no significant change was observed in the control group (Supplemental Material Fig. 1B).

3.3. Biocompatibility of myocardial dECM

To determine whether cells could grow in the myocardial dECM, ADSCs were seeded in three different concentrations of myocardial dECM at a density of 5×10^5 cells/well in six well plates. ADSCs could adhere, extend, and survive in myocardial dECM. However, there was a significant difference in the growth and proliferation of ADSCs in the three different myocardial dECM concentrations. As shown in Fig. 2A–C, ADSC growth was observed in the middle zone of the 1.5% and 2.5% myocardial dECM along with some dead cells, while cells were evenly distributed in 2.0% myocardial dECM with few dead cells after 3 days probably due to the even aperture and microstructure arrangement. As shown in Fig. 2D–F, after incubation for 7 days, although cells were uniformly distributed in 1.5% myocardial dECM, they were few in number. There were some clustered cells in 2.5% myocardial dECM, which may be related to the dense apertures in higher dECM concentrations. However, the data showed that ADSCs could fully extend and were evenly distributed in 2.0% myocardial dECM, which indicated that 2.0% was the optimum concentration. In addition, according to the proliferation curve, ADSC growth was the fastest in the 2.0% myocardial dECM (Fig. 2G). Hence, the 2.0% myocardial dECM was selected for further experiments.

3.4. ADSCs combined with myocardial dECM increased angiogenesis in MI rats

Timely reconstruction of blood supply is beneficial for the recovery of cardiac function. The data from this study demonstrated that the mRNA expression level of Ang-1, VEGF, and EGF was significantly increased in the dECM + ADSCs group compared with the other groups 4 weeks after treatment (Fig. 3A–C). Moreover, the protein expression of Ang-1, VEGF, and EGF was slightly elevated in the ADSCs and dECM group, but obviously increased in the dECM + ADSCs group (Fig. 3D–G), which was consistent with the relative mRNA expression. The mRNA and protein expression were higher in the sham group than in the MI group, and the reason may be that infarct injury decreased the expression of angiogenesis-related factors. Most importantly, the combination group showed the significant higher mean number of vessels than that of the other groups (Fig. H, I). These results indicated that ADSCs combined with myocardial dECM could increase angiogenesis

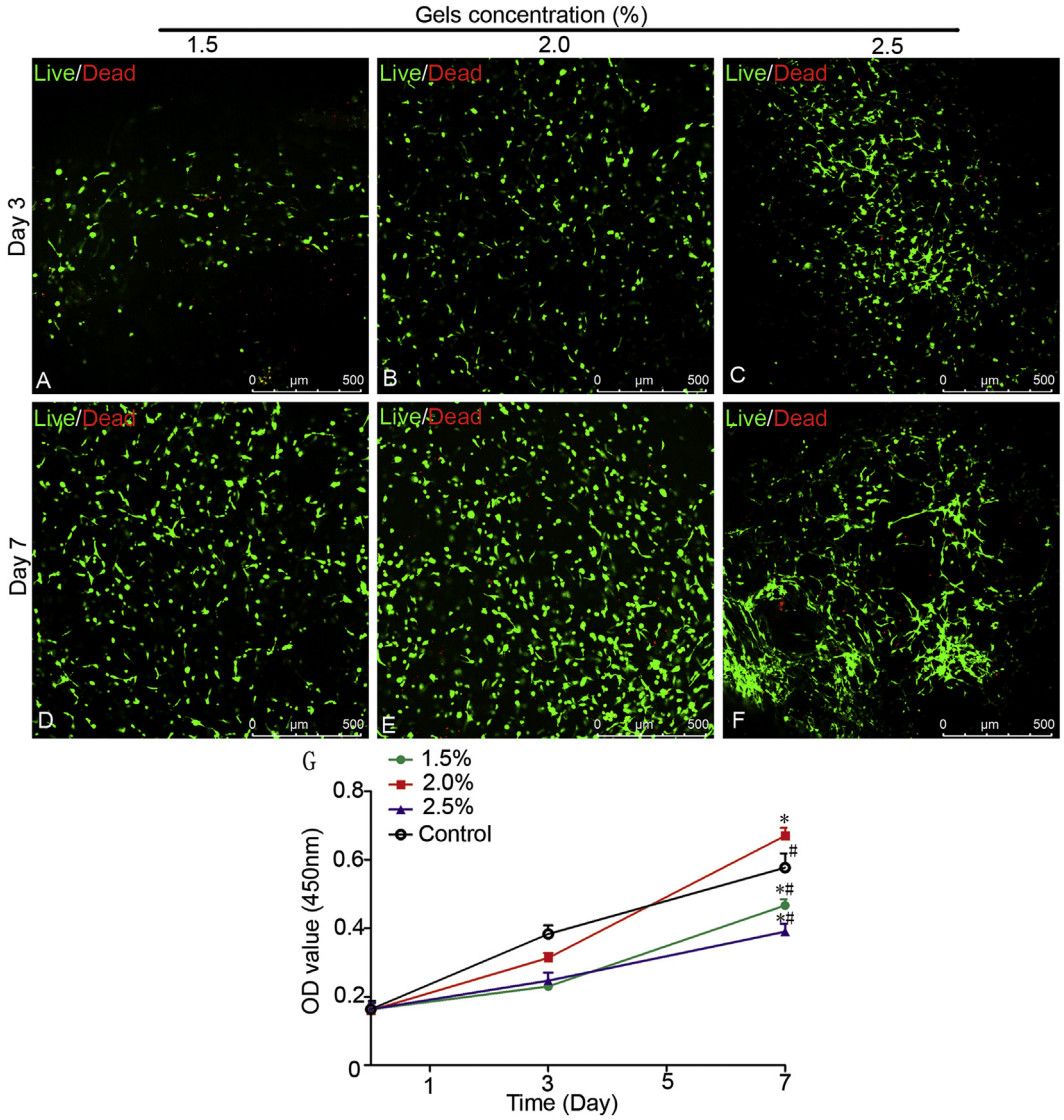

Fig. 2. The growth and proliferation of ADSCs seeded in three different concentrations of myocardial dECM. **A-C.** Proliferation of ADSCs seeded in 1.5%, 2.0%, and 2.5% myocardial dECM for 3 days. **D-F.** Proliferation of ADSCs seeded in 1.5%, 2.0%, and 2.5% myocardial dECM for 7 days. **G.** Proliferation curve of ADSCs seeded in myocardial dECM for 0, 3 and 7 days. Scale bar = 500 μm. Control, ADSCs seeded without myocardial dECM (*P < 0.05 vs. Control, #P < 0.05 vs. 2.0%).

more efficiently, which can provide the blood supply for the recovery of cardiac function.

3.5. Morphological changes in the heart of MI rats after treatment with ADSCs combined with myocardial dECM

To evaluate the effect of ADSCs combined with myocardial dECM on fibrosis *in vivo*, Masson's trichrome staining was performed to investigate cardiac histology at 4 weeks post-injection. Severe fibrosis (blue) of the left ventricle could be clearly distinguished from the normal myocardium (red) in the MI group. After treatment for 4 weeks, the fibrosis in the infarct zone was slightly decreased in the ADSCs and dECM group. The least collagen fiber deposition was in the dECM + ADSCs group, suggesting that most scar tissues may have been replaced by normal myocardial tissues after the combination treatment (Fig. 3J and K).

Infarct size was calculated and analyzed by TTC staining. The infarct size slightly decreased to (34.2 ± 2.3%) and (43.3 ± 1.7%) in the ADSCs and dECM group, respectively. The most significant reduction was in the dECM + ADSCs group (24 ± 1.4%) compared with the MI group (58.3 ± 2.9%). The data indicated that the combination of ADSCs and myocardial dECM could reduce infarct size significantly, which yielded synergistic effects (Fig. 3L, M).

3.6. ADSCs combined with myocardial dECM ameliorated cardiac function in MI rat model

The deterioration of cardiac function after MI may be due to the interruption of the blood supply and the following negative progressive remodeling of the left ventricle. The cardiac function was investigated by echocardiography at 4 weeks after treatment. As shown in Fig. 3N, MI rats showed typical cardiac ultrasonography after infarct injury. The LVIDd and LVIDs increased significantly, while LVEF and LVFS obviously decreased in the MI group compared with the sham group. The LVIDd and LVIDs decreased in the pure dECM and ADSCs group compared with the MI group, which indicated slight recovery of cardiac function. Importantly, LVEF was augmented to 55.4 ± 2.8% and 47 ± 2% in the ADSCs and dECM group, respectively. The increase was most obvious in combined group (68.8 ± 5.6%) compared with the MI group (29.4 ± 1.2%), suggesting that the injection of ADSCs with myocardial dECM could effectively enhance cardiac function.

In addition, hemodynamic evaluation demonstrated that the +dp/

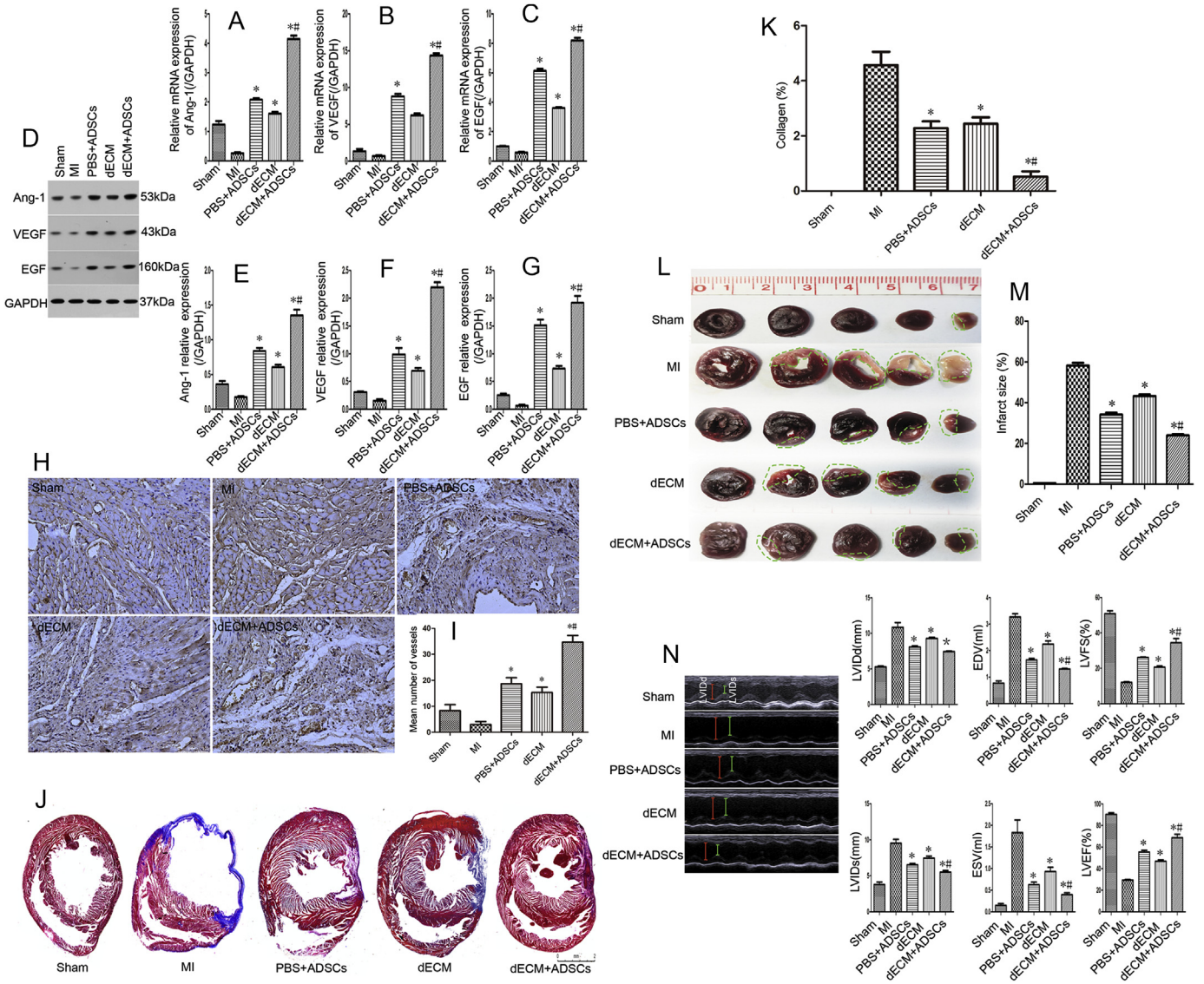

Fig. 3. A-C. Relative mRNA expression of Ang-1, VEGF, and EGF (n = 3/group). **D.** Representative western blot images showing the protein levels of Ang-1, VEGF and EGF. **E-G.** Quantitative analysis of Ang-1, VEGF, and EGF protein expression (n = 3/group). **H.** Immunohistochemistry with vWF staining 4 weeks after treatment. Scar bar = 100 μm. **I.** Quantitative analysis of the mean number of vessels. **J.** Masson's trichrome staining images of treated hearts 4 weeks after treatment. **K.** Quantitative analysis of the ratio of collagen by Masson's trichrome staining (n = 3/group). **L.** TTC staining of different groups for infarct size 4 weeks after treatment. The pale white area (green dotted line area) represents the infarct zone, and the darker red area is the normal myocardial tissue. **M.** Quantitative analysis of infarct size after MI (n = 6/group). **N.** Representative echocardiography images for assessment of cardiac function 4 weeks after treatment *in vivo* (n = 3/group). (*P < 0.05 vs. MI, #P < 0.05 vs. PBS + ADSCs). (For interpretation of the references to color in this figure legend, the reader is referred to the Web version of this article.)

Table 2
Hemodynamic evaluation of cardiac function 4 weeks post treatment (mmHg/s).

	Sham	MI	PBS + ADSCs	dECM	dECM + ADSCs
+dp/dtmax	4363 ± 362	2230 ± 270	3360 ± 205*	2787 ± 266*	3683 ± 282*#
-dp/dtmin	4052 ± 289	1986 ± 255	3156 ± 225*	2556 ± 232*	3498 ± 276*#

+dp/dt max, peak rate of pressure rise; -dp/dt min, peak rate of pressure decline. n = 7/group (*P < 0.05 vs MI, #P < 0.05 vs PBS + ADSCs).

dt max (peak rate of pressure rise) and -dp/dt min (peak rate of pressure decline) in the dECM and ADSCs group improved slightly compared with the MI group, suggesting that there was little recovery in hemodynamics after treatment. The data indicated that the +dp/dt max in the dECM + ADSCs group (3683 ± 282) was higher than that in the MI group (2230 ± 270), and the -dp/dt min in the dECM + ADSCs group (3498 ± 276) also increased compared with the MI group (1986 ± 255) (Table 2).

4. Discussion

In this study, we confirmed the hypothesis that the combination of ADSCs and myocardial dECM could alleviate myocardial damage and improve cardiac function after acute MI, which further proves that the

combination of biomaterials and stem cells is increasingly effective in the treatment of myocardial ischemia. Biomaterials can provide a relatively protective three-dimensional microenvironment for stem cells, and the combined therapy is more effective. Arana et al. [29] confirmed that a collagen sponge combined with ADSCs could greatly improve graft cell survival rate and therapeutic effect. ADSCs implanted into chitosan hydrogels for MI treatment have been shown to significantly ameliorate cardiac function compared with pure cell transplantation [30]. Also, a π-π conjugation-containing soft and conductive injectable polymer hydrogel encapsulating ADSCs not only promoted the transmission of mechanical and electrical signals, but also improved heart function after MI in rats [31]. Compared with other biomaterials, dECM has unique advantages, such as better biocompatibility and a more suitable three-dimensional environment. We investigated the cell viability and proliferation of ADSCs at different times after seeding into myocardial dECM. The results indicated that myocardial dECM had good biocompatibility, which corresponded with findings from previous studies. Christman KL et al. [32] reported that the myocardial dECM hydrogel can offer a cardiac-specific extracellular environment and does not cause an immune reaction. Falguni P et al. [33] developed a bioprinting process using heart tissue dECM bioinks capable of providing crucial cues for cell engraftment. We improved the method for myocardial dECM preparation based on previous protocols [17]. The digestion time was shortened from 48 h to only 6 h by increasing the temperature from room temperature to 35.5 °C [34]. Myocardial dECM can act as a scaffold, which may be closely related to the composition of the hydrogel. ECM components are complex, including type I collagen, III collagen, silk protein, laminin, cellulose and chitosan [35]. Singelyn et al. [17] confirmed, using gel electrophoresis, that there are several kinds of small molecular substances in decellularized extracellular matrix of myocardium, and collagen accounts for a large proportion. We further detected the main components after decellularization and ensured that there was no obvious change in laminin, and types I and III collagen compared with normal myocardial tissues.

ADSCs encapsulated into myocardial dECM exerted enhanced effects. Combination therapy could inhibit scar formation, improve ventricular remodeling, and enhance the recovery of LV function. These effects can be interpreted based on the following facts. Firstly, myocardial dECM itself can promote tissue repair. Singelyn et al. confirmed that the injection of acellular matrix could promote angiogenesis and cardiomyocyte survival in the infarct area. Morris et al. [36] found that a mouse skin-derived decellularized matrix promoted angiogenesis around diabetic wounds and accelerated wound healing. Our results showed that myocardial dECM could increase the expression of angiogenesis-related factors and the mean number of vessels. In addition, myocardial dECM could mimic the biological and chemical cues of the native myocardial ECM, cross-talk with resident cells and affect reparative processes [27]. Sarig et al. indicated that a decellularized porcine cardiac extracellular matrix (pcECM) patch could improve cardiac function, and the mechanism was related to the recruited progenitors that differentiated into CM-like cells. Jennifer et al. [37] demonstrated that the injection of the dECM could increase endogenous cardiomyocytes in the infarct area and maintain cardiac function without inducing arrhythmias in rat MI. Secondly, ADSCs could secrete a large number of cytokines in hypoxic environment, such as interleukin-1, VEGF, fibroblast growth factor-2, and transformed growth factor-β, which have been shown to improve the injured microenvironment and enhanced the viability of cells to resist hypoxia in the infarcted area [38,39]. Our data demonstrated that the mean number of vessels was higher in the ADSCs group than the MI group, which may be related to the paracrine function of ADSCs. Cai et al. [40] demonstrated that human-derived ADSCs promote cardiac function recovery after MI by inducing angiogenesis. Thirdly, scaffold materials can reduce ventricular wall pressure for transplanted cells to some extent. The Young's modulus of the native human heart varies from 0.02 to 0.50 MPa depending on whether the heart is in systole or diastole [41]. Although the myocardial dECM did not achieve the Young's modulus of native heart tissue, it could protect ADSCs by limiting direct contact with the injured tissues.

In summary, the findings of the study demonstrated that ADSCs combined with myocardial dECM could significantly promote the therapeutic effect on acute MI rats, and the underlying mechanism may be related to the dual effect of ADSCs and myocardial dECM. There were also some limitations in this study, such as not tracking ADSCs during the treatment process.

5. Conclusion

In the study, the preparation process of injectable myocardial dECM was optimized, and the fabrication time was greatly shortened. We focus on the synergistic effects of ADSCs and myocardial dECM after acute MI. The results showed that ADSCs encapsulated in myocardial dECM reduced fibrosis and infarct size, and significantly improve the recovery of cardiac function. The mechanism may be closely related to the increasing angiogenesis, which further promote the recovery of cardiac function. Myocardial dECM as support is helpful in the regeneration of the infarcted cardiac tissue. Future studies will be focus on elucidating the specific mechanism by which the myocardial dECM protects transplanted cells from the harmful environment in the infarct area.

Ethics approval

All animals were permitted by the Animal Care and Use Committee of the Second Military Medical University (permit number SYXK-2002-042).

Availability of data and materials

All data generated and/or analyzed during this study are included in this published article.

Conflicts of interest

The authors declare that they have no competing interests.

Author's contributions

Liang Qiao (1719415708@qq.com), Yingshen Shi (aerosys@live.com) and Yan Kong (kongyan420@163.com) performed the research. Yan Kong analyzed data and wrote the paper. Aijun Sun performed the histological staining. Ruijuan Ji gave suggestions. Chao Huang performed the western blotting. Yuquan Li and Xiangqun Yang designed this study and gave suggestions. All authors read and approved the final manuscript.

Funding

This work was supported by the Funds of the National Natural Science Foundation of China (31271050) and the Funds of Anhui Medical University (2018xkj003).

Declaration of competing interest

Not applicable.

Acknowledgements

We thank Liang-Hua Wang from Naval Medical University for his technical assistance in freeze-drying.

Appendix A. Supplementary data

Supplementary data to this article can be found online at https://doi.org/10.1016/j.lfs.2019.116891.

Abbreviations

MI	Acute myocardial infarction
BSA	Bovine serum albumin
DMEM	Dulbecco's modified Eagle's medium
ECG	Electrocardiography
MI	Myocardial infarction
LAD	Left anterior descending artery
LV	Left ventricular
PCR	Polymerase chain reaction
IL	Interleukin
TNF-α	tumor necrosis factor alpha
ELISA	Enzyme-linked immunosorbent assay
TTC	2,3,5-Triphenyl-tetrazolium chloride
Ang-1	angiopoietin-1
VEGF	vascular endothelial growth factor
EGF	epidermal growth factor

References

[1] F. Lee, P. Maggiore, K. Chung, Self-management of an inferior ST-segment elevation myocardial infarction, N. Engl. J. Med. 378 (2018) 960–962, https://doi.org/10.1056/NEJMc1716701.

[2] A.S. Go, D. Mozaffarian, V.L. Roger, E.J. Benjamin, J.D. Berry, M.J. Blaha, S. Dai, E.S. Ford, C.S. Fox, S. Franco, H.J. Fullerton, C. Gillespie, S.M. Hailpern, J.A. Heit, V.J. Howard, M.D. Huffman, S.E. Judd, B.M. Kissela, S.J. Kittner, D.T. Lackland, J.H. Lichtman, L.D. Lisabeth, R.H. Mackey, D.J. Magid, G.M. Marcus, A. Marelli, D.B. Matchar, D.K. McGuire, E.R. Mohler 3rd, C.S. Moy, M.E. Mussolino, R.W. Neumar, G. Nichol, D.K. Pandey, N.P. Paynter, M.J. Reeves, P.D. Sorlie, J. Stein, A. Towfighi, T.N. Turan, S.S. Virani, N.D. Wong, D. Woo, M.B. Turner, Executive summary: heart disease and stroke statistics–2014 update: a report from the American Heart Association, Circulation 129 (2014) 399–410, https://doi.org/10.1161/01.cir.0000442015.53336.12.

[3] P. Nigro, B. Bassetti, L. Cavallotti, V. Catto, C. Carbucicchio, G. Pompilio, Cell therapy for heart disease after 15 years: unmet expectations, Pharmacol. Res. 127 (2018) 77–91, https://doi.org/10.1016/j.phrs.2017.02.015.

[4] H.S. Bernstein, D. Srivastava, Stem cell therapy for cardiac disease, Pediatr. Res. 71 (2012) 491–499, https://doi.org/10.1038/pr.2011.61.

[5] C. Chi, F. Wang, B. Xiang, J. Deng, S. Liu, H.Y. Lin, K. Natarajan, G. Li, L. Wang, J. Wang, F. Lin, D.H. Freed, R.C. Arora, H. Liu, G. Tian, Adipose-derived stem cells from both visceral and subcutaneous fat deposits significantly improve contractile function of infarcted rat hearts, Cell Transplant. 24 (2015) 2337–2351, https://doi.org/10.3727/096368914x685780.

[6] T. Ma, J. Sun, Z. Zhao, W. Lei, Y. Chen, X. Wang, J. Yang, Z. Shen, A brief review: adipose-derived stem cells and their therapeutic potential in cardiovascular diseases, Stem Cell Res. Ther. 8 (2017) 124, https://doi.org/10.1186/s13287-017-0585-3.

[7] M. Gautam, D. Fujita, K. Kimura, H. Ichikawa, A. Izawa, M. Hirose, T. Kashihara, M. Yamada, M. Takahashi, U. Ikeda, Y. Shiba, Transplantation of adipose tissue-derived stem cells improves cardiac contractile function and electrical stability in a rat myocardial infarction model, J. Mol. Cell. Cardiol. 81 (2015) 139–149, https://doi.org/10.1016/j.yjmcc.2015.02.012.

[8] J. Bobi, N. Solanes, R. Fernandez-Jimenez, C. Galan-Arriola, A.P. Dantas, L. Fernandez-Friera, C. Galvez-Monton, E. Rigol-Monzo, J. Aguero, J. Ramirez, M. Roque, A. Bayes-Genis, J. Sanchez-Gonzalez, A. Garcia-Alvarez, M. Sabate, S. Roura, B. Ibanez, M. Rigol, Intracoronary administration of allogeneic adipose tissue-derived mesenchymal stem cells improves myocardial perfusion but not left ventricle function, in a translational model of acute myocardial infarction, J. Am. Heart Assoc. 6 (2017), https://doi.org/10.1161/JAHA.117.005771.

[9] H. Wang, J. Shi, Y. Wang, Y. Yin, L. Wang, J. Liu, Z. Liu, C. Duan, P. Zhu, C. Wang, Promotion of cardiac differentiation of brown adipose derived stem cells by chitosan hydrogel for repair after myocardial infarction, Biomaterials 35 (2014) 3986–3998, https://doi.org/10.1016/j.biomaterials.2014.01.021.

[10] Q. Liu, S. Tian, C. Zhao, X. Chen, I. Lei, Z. Wang, P.X. Ma, Porous nanofibrous poly (L-lactic acid) scaffolds supporting cardiovascular progenitor cells for cardiac tissue engineering, Acta Biomater. 26 (2015) 105–114, https://doi.org/10.1016/j.actbio.2015.08.017.

[11] L. Wang, E.M. Meier, S. Tian, I. Lei, L. Liu, S. Xian, M.T. Lam, Z. Wang, Transplantation of Isl1(+) cardiac progenitor cells in small intestinal submucosa improves infarcted heart function, Stem Cell Res. Ther. 8 (2017) 230, https://doi.org/10.1186/s13287-017-0675-2.

[12] P. Díaz-Herráez, L. Saludas, S. Pascual-Gil, T. Simón-Yarza, G. Abizanda, F. Prósper, E. Garbayo, M.J. Blanco-Prieto, Transplantation of adipose-derived stem cells combined with neuregulin-microparticles promotes efficient cardiac repair in a rat myocardial infarction model, J. Control. Release 249 (2017) 23–31, https://doi.org/10.1016/j.jconrel.2017.01.026.

[13] K.A. Kyburz, K.S. Anseth, Synthetic mimics of the extracellular matrix: how simple is complex enough? Ann. Biomed. Eng. 43 (2015) 489–500, https://doi.org/10.1007/s10439-015-1297-4.

[14] Y. Eitan, U. Sarig, N. Dahan, M. Machluf, Acellular cardiac extracellular matrix as a scaffold for tissue engineering: in vitro cell support, remodeling, and biocompatibility, Tissue Eng. C Methods 16 (2010) 671–683, https://doi.org/10.1089/ten.TEC.2009.0111.

[15] U. Sarig, G.C. Au-Yeung, Y. Wang, T. Bronshtein, N. Dahan, F.Y. Boey, S.S. Venkatraman, M. Machluf, Thick acellular heart extracellular matrix with inherent vasculature: a potential platform for myocardial tissue regeneration, Tissue Eng. A 18 (2012) 2125–2137, https://doi.org/10.1089/ten.TEA.2011.0586.

[16] U. Sarig, E.B. Nguyen, Y. Wang, S. Ting, T. Bronshtein, H. Sarig, N. Dahan, M. Gvirtz, S. Reuveny, S.K. Oh, T. Scheper, Y.C. Boey, S.S. Venkatraman, M. Machluf, Pushing the envelope in tissue engineering: ex vivo production of thick vascularized cardiac extracellular matrix constructs, Tissue Eng. A 21 (2015) 1507–1519, https://doi.org/10.1089/ten.TEA.2014.0477.

[17] J.M. Singelyn, J.A. DeQuach, S.B. Seif-Naraghi, R.B. Littlefield, P.J. Schup-Magoffin, K.L. Christman, Naturally derived myocardial matrix as an injectable scaffold for cardiac tissue engineering, Biomaterials 30 (2009) 5409–5416, https://doi.org/10.1016/j.biomaterials.2009.06.045.

[18] Y.D. Lin, M.L. Yeh, Y.J. Yang, D.C. Tsai, T.Y. Chu, Y.Y. Shih, M.Y. Chang, Y.W. Liu, A.C. Tang, T.Y. Chen, C.Y. Luo, K.C. Chang, J.H. Chen, H.L. Wu, T.K. Hung, P.C. Hsieh, Intramyocardial peptide nanofiber injection improves postinfarction ventricular remodeling and efficacy of bone marrow cell therapy in pigs, Circulation 122 (2010) S132–S141, https://doi.org/10.1161/CIRCULATIONAHA.110.939512.

[19] T. Shimizu, M. Yamato, A. Kikuchi, T. Okano, Cell sheet engineering for myocardial tissue reconstruction, Biomaterials 24 (2003) 2309–2316.

[20] Q. Li, Y. Yin, Y. Zheng, F. Chen, P. Jin, Inhibition of autophagy promoted high glucose/ROS-mediated apoptosis in ADSCs, Stem Cell Res. Ther. 9 (2018) 289, https://doi.org/10.1186/s13287-018-1029-4.

[21] X. Zhang, J. Qin, X. Wang, X. Guo, J. Liu, X. Wang, X. Wu, X. Lu, W. Li, X. Liu, Netrin-1 improves adipose-derived stem cell proliferation, migration, and treatment effect in type 2 diabetic mice with sciatic denervation, Stem Cell Res. Ther. 9 (2018) 285, https://doi.org/10.1186/s13287-018-1020-0.

[22] Y. Song, C. Zhang, J. Zhang, N. Sun, K. Huang, H. Li, Z. Wang, K. Huang, L. Wang, An injectable silk sericin hydrogel promotes cardiac functional recovery after ischemic myocardial infarction, Acta Biomater. 41 (2016) 210–223, https://doi.org/10.1016/j.actbio.2016.05.039.

[23] C. Shen, Q. Quan, C. Yang, Y. Wen, H. Li, Histone demethylase JMJD6 regulates cellular migration and proliferation in adipose-derived mesenchymal stem cells, Stem Cell Res. Ther. 9 (2018) 212, https://doi.org/10.1186/s13287-018-0949-3.

[24] Y. Li, L. Wang, Z. Dong, S. Wang, L. Qi, K. Cho, Z. Zhang, N. Li, Y. Hu, B. Jiang, Cardioprotection of salvianolic acid B and ginsenoside Rg1 combination on subacute myocardial infarction and the underlying mechanism, Phytomedicine : Int. J. Phytother. Phytopharm. 57 (2019) 255–261, https://doi.org/10.1016/j.phymed.2018.12.040.

[25] R. Chen, X. Cai, J. Liu, B. Bai, X. Li, Sphingosine 1-phosphate promotes mesenchymal stem cell-mediated cardioprotection against myocardial infarction via ERK1/2-MMP-9 and Akt signaling axis, Life Sci. 215 (2018) 31–42, https://doi.org/10.1016/j.lfs.2018.10.047.

[26] S. Cheng, X. Zhang, Q. Feng, J. Chen, L. Shen, P. Yu, L. Yang, D. Chen, H. Zhang, W. Sun, X. Chen, Astragaloside IV exerts angiogenesis and cardioprotection after myocardial infarction via regulating PTEN/PI3K/Akt signaling pathway, Life Sci. 227 (2019) 82–93, https://doi.org/10.1016/j.lfs.2019.04.040.

[27] U. Sarig, H. Sarig, E. de-Berardinis, S.Y. Chaw, E.B. Nguyen, V.S. Ramanujam, V.D. Thang, M. Al-Haddawi, S. Liao, D. Seliktar, T. Kofidis, F.Y. Boey, S.S. Venkatraman, M. Machluf, Natural myocardial ECM patch drives cardiac progenitor based restoration even after scarring, Acta Biomater. 44 (2016) 209–220, https://doi.org/10.1016/j.actbio.2016.08.031.

[28] Q. Ma, J. Yang, X. Huang, W. Guo, S. Li, H. Zhou, J. Li, F. Cao, Y. Chen, Poly (Lactide-Co-Glycolide)-Monomethoxy-Poly-(Polyethylene glycol) nanoparticles loaded with melatonin protect adipose-derived stem cells transplanted in infarcted heart tissue, Stem Cells 36 (2018) 540–550, https://doi.org/10.1002/stem.2777.

[29] M. Arana, E. Pena, G. Abizanda, M. Cilla, I. Ochoa, J.J. Gavira, G. Espinosa, M. Doblare, B. Pelacho, F. Prosper, Preparation and characterization of collagen-based ADSC-carrier sheets for cardiovascular application, Acta Biomater. 9 (2013) 6075–6083, https://doi.org/10.1016/j.actbio.2012.12.014.

[30] Z. Liu, H. Wang, Y. Wang, Q. Lin, A. Yao, F. Cao, D. Li, J. Zhou, C. Duan, Z. Du, Y. Wang, C. Wang, The influence of chitosan hydrogel on stem cell engraftment, survival and homing in the ischemic myocardial microenvironment, Biomaterials 33 (2012) 3093–3106, https://doi.org/10.1016/j.biomaterials.2011.12.044.

[31] R. Bao, B. Tan, S. Liang, N. Zhang, W. Wang, W. Liu, A pi-pi conjugation-containing soft and conductive injectable polymer hydrogel highly efficiently rebuilds cardiac function after myocardial infarction, Biomaterials 122 (2017) 63–71, https://doi.org/10.1016/j.biomaterials.2017.01.012.

[32] K.L. Christman, R.J. Lee, Biomaterials for the treatment of myocardial infarction, J. Am. Coll. Cardiol. 48 (2006) 907–913, https://doi.org/10.1016/j.jacc.2006.06.005.

[33] F. Pati, J. Jang, D.H. Ha, S. Won Kim, J.W. Rhie, J.H. Shim, D.H. Kim, D.W. Cho, Printing three-dimensional tissue analogues with decellularized extracellular matrix bioink, Nat. Commun. 5 (2014) 3935, https://doi.org/10.1038/ncomms4935.

[34] J. Jang, H.J. Park, S.W. Kim, H. Kim, J.Y. Park, S.J. Na, H.J. Kim, M.N. Park,

S.H. Choi, S.H. Park, S.W. Kim, S.M. Kwon, P.J. Kim, D.W. Cho, 3D printed complex tissue construct using stem cell-laden decellularized extracellular matrix bioinks for cardiac repair, Biomaterials 112 (2017) 264–274.

[35] Y. Efraim, H. Sarig, N. Cohen Anavy, U. Sarig, E. de Berardinis, S.Y. Chaw, M. Krishnamoorthi, J. Kalifa, H. Bogireddi, T.V. Duc, T. Kofidis, L. Baruch, F.Y.C. Boey, S.S. Venkatraman, M. Machluf, Biohybrid cardiac ECM-based hydrogels improve long term cardiac function post myocardial infarction, Acta Biomater. 50 (2017) 220–233, https://doi.org/10.1016/j.actbio.2016.12.015.

[36] A.H. Morris, D.K. Stamer, B. Kunkemoeller, J. Chang, H. Xing, T.R. Kyriakides, Decellularized materials derived from TSP2-KO mice promote enhanced neovascularization and integration in diabetic wounds, Biomaterials 169 (2018) 61–71, https://doi.org/10.1016/j.biomaterials.2018.03.049.

[37] J.M. Singelyn, P. Sundaramurthy, T.D. Johnson, P.J. Schup-Magoffin, D.P. Hu, D.M. Faulk, J. Wang, K.M. Mayle, K. Bartels, M. Salvatore, A.M. Kinsey, A.N. Demaria, N. Dib, K.L. Christman, Catheter-deliverable hydrogel derived from decellularized ventricular extracellular matrix increases endogenous cardiomyocytes and preserves cardiac function post-myocardial infarction, J. Am. Coll. Cardiol. 59 (2012) 751–763, https://doi.org/10.1016/j.jacc.2011.10.888.

[38] S. Banai, M.T. Jaklitsch, M. Shou, D.F. Lazarous, M. Scheinowitz, S. Biro, S.E. Epstein, E.F. Unger, Angiogenic-induced enhancement of collateral blood flow to ischemic myocardium by vascular endothelial growth factor in dogs, Circulation 89 (1994) 2183–2189.

[39] V. Planat-Benard, C. Menard, M. Andre, M. Puceat, A. Perez, J.M. Garcia-Verdugo, L. Penicaud, L. Casteilla, Spontaneous cardiomyocyte differentiation from adipose tissue stroma cells, Circ. Res. 94 (2004) 223–229, https://doi.org/10.1161/01.RES.0000109792.43271.47.

[40] L. Cai, B.H. Johnstone, T.G. Cook, J. Tan, M.C. Fishbein, P.S. Chen, K.L. March, IFATS collection: human adipose tissue-derived stem cells induce angiogenesis and nerve sprouting following myocardial infarction, in conjunction with potent preservation of cardiac function, Stem Cells 27 (2009) 230–237, https://doi.org/10.1634/stemcells.2008-0273.

[41] M. Kapnisi, C. Mansfield, C. Marijon, A.G. Guex, F. Perbellini, I. Bardi, E.J. Humphrey, J.L. Puetzer, D. Mawad, D.C. Koutsogeorgis, D.J. Stuckey, C.M. Terracciano, S.E. Harding, M.M. Stevens, Auxetic cardiac patches with tunable mechanical and conductive properties toward treating myocardial infarction, Adv. Funct. Mater. 28 (2018) 1800618, https://doi.org/10.1002/adfm.201800618.